01,14

Behavior of magnesium alloy Mg-9Gd-4Y-1Zn-0.5Zr in the wide range of strain rate

© S.A. Atroshenko[1,2], M.N. Antonova[1,2], S. Zhao[2], L. Xu[2], R.V. Lukashov[2], Yu.V. Petrov[1,2]

[1] Institute for Problems in Mechanical Engineering of the Russian Academy of Sciences, St. Petersburg, Russia
[2] St. Petersburg State University, St. Petersburg, Russia

E-mail: satroshe@mail.ru

Received September 23, 2025
Revised October 17, 2025
Accepted October 17, 2025

In this paper, we study the magnesium alloy Mg-9Gd-4Y-1Zn-0.5Zr (wt.%), which was obtained by direct die casting with cooling and subsequent homogenization at 510 °C for 12 h and quenching in water. Then, the alloy was extruded at 350 °C with an extrusion ratio of 10 and a plunger speed of 1 mm/s. Static tests of the alloy were performed on an Instron machine at two strain rates: $10^{-3}\,s^{-1}$ and $10^{-1}\,s^{-1}$. Dynamic studies were carried out using the Taylor and Hopkinson methods. An analysis of changes in the characteristics and microstructure of this alloy was carried out in the strain rate range covering both static and dynamic loading rates. Micromechanisms of deformation and fracture of the magnesium alloy were identified.

Keywords: magnesium alloy, static and dynamic loading, micromechanisms of deformation and fracture.

DOI: 10.61011/PSS.2025.10.62622.261-25

1. Introduction

Magnesium alloys are of great interest to the researchers because of low density of these alloys compared to other metals, which can be used in the automotive and aerospace industries to reduce the weight of devices. Rare-earth magnesium alloys alloyed with gadolinium (Gd), yttrium (Y), zinc (Zn) and zirconium (Zr) are of particular interest due to their high potential in areas requiring a combination of high strength and thermal stability [1]. Among the alloys of this group is Mg-9Gd-4Y-1Zn-0.5Zr alloy (mass.%), belonging to Mg-*RE*-Zn-Zr system, where *RE* — is a rare earth element, is widely studied as the basis for new generation structural materials. After hot extrusion, the alloy structure is characterized by the predominant formation of a lamellar phase with a long-period stacking ordered (LPSO), which is formed mainly along the direction of deformation. These phases may exist both, in the form of particles extended along the extrusion line, and as the intra-crystalline inclusions, especially in case of high concentrations of Zn and rare earth elements. The presence of LPSO phases contributes to the reinforcement of the matrix and increases slip and shear resistance, which results in improved strength characteristics. For example, in Mg-10Gd-3Y-1.5Zn-0.5Zr alloys, a continuous set of lamellar LPSO and minor stacking faults (SF) was found inside the grains, which ensures high tensile strength even at temperatures up to 300 °C [2].

Extrusion also promotes the development of dynamic recrystallization, leading to the formation of equiaxed grains ($\sim 1-5\,\mu m$) with their size varying depending on the conditions of deformation and preliminary heat treatment. Zr plays an additional role in recrystallization, ensuring the formation of new grains and limiting their growth due to its tendency to heterogeneous distribution along grain boundaries [3].

Since solubility of Gd and Y in the solid solution of α-Mg matrix strongly depends on the temperature, the degree of ordering during aging may be regulated by release of β'-phase (metastable release of Mg-Gd/Y) [4]. Formation of LPSO phases and release of γ' (metastable release of Mg-Gd/Y-Zn) occur as a result of adding Zn atoms to Mg-Gd-Y alloys [5].

In the present study, an extruded Mg-9Gd-4Y-1Zn-0.5Zr alloy (mass.%) was studied fabricated by direct injection molding with cooling, followed by homogenization at 510 °C for 12 h and quenching in water [6]. The alloy was then extruded into bars at 350 °C with an extrusion coefficient of 10 at a constant plunger speed of 1 mm/s. Tensile tests conducted by the authors of [6] gave the values of yield strength, tensile strength and elongation before fracture of this alloy, which were 323 and 381 MPa and 15.1 %, respectively.

2. Material and research techniques

The specimens of Mg-9Gd-4Y-1Zn-0.5Zr alloy (mass.%) were fabricated by extrusion at a constant plunger speed of 1 mm/s and cut in its direction.

2.1. Study of microstructure

The microstructure was studied using Axio Observer Z1M optical microscope in a light field using a circular polarization differentiation interference contrast (C_DIC); the amount of viscous component on the fracture surface was determined in a dark field according to ASTM E436-03 using an Axio Vision image analyzer, as well as using a scanning electron microscope Zeiss Merlin. The chemical composition was studied by energy dispersive spectroscopy (EDS, EDX), thanks to the provision of a microscope with an additional attachment for X-ray microanalysis by Oxford InstrumentsINCAx-act. The microhardness of the transverse sections was measured with applied load of 100 g using SHIMADZU device of grade HMV-G.

2.2. Loading mode

The specimens were tested using three testing layouts: static compression, split Hopkinson pressure bar test and Taylor test. All the experiments were carried out with the compression load applied. Quasi-static compression studies were carried out using Instron testing machine (strain rates 10^{-1} and $10^{-3}\,s^{-1}$). Dynamic tests were performed using Hopkinson–Kolsky method (strain rates from 1300 to $5970\,s^{-1}$) and the Taylor test.

The initial cylindrical specimens with a diameter of 8 mm were cut using ARTA 153 PRO electrical discharge machine. Thus, in all tests, the loading axis coincided with the direction of extrusion of the studied magnesium alloy. In Taylor tests the cylinders 8 mm in diameter and 30 mm long were used, in Hopkinson test — cylinders $D = 8$ mm in diameter and $L = 4$ mm ($L/D = 1/2$) long; for static tests — cylinders 8 mm in diameter and 8 mm ($L/D = 1$) long. Before testing, the ends of all specimens were ground.

2.2.1. Split Hopkinson pressure bar tests

A series of experiments using a split Hopkinson pressure bar (SHPB) was conducted to study the characteristics and mechanisms of destruction of the tested micro-material under dynamic compression.

The selected geometry of the specimen ($D = 8$ mm, $L = 4$ mm) provided conditions for a uniform and flat stress state, while providing enough material volume to determine microstructural characteristics after testing.

The length of the falling and transmitting bars was 2 m, diameter — 20 mm. All system components were made of the high-strength steel (Young's modulus $E = 226$ GPa). The loading pulse was created by an impactor with a length of 60 cm. The impactor was accelerated using a pneumatic system with pressure control in the chamber in the range from 3 to 6 atm. The corresponding impact velocities measured using a laser velocimeter ranged from 3.7 to 11 m/s, resulting in deformation rates of approximately 800 to $6000\,s^{-1}$.

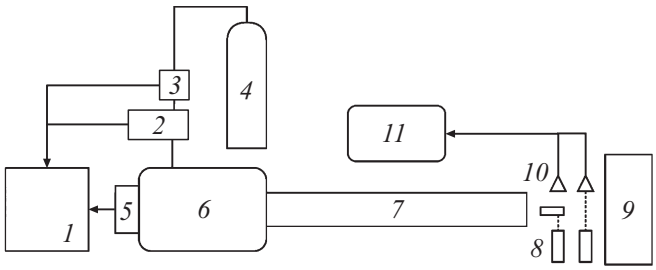

Figure 1. Experimental setup. *1* — microcontroller, *2* — pressure sensor, *3* — high pressure valve, *4* — gas cylinder, *5* — trigger, *6* — pressure chamber, *7* — gun barrel, *8* — lasers, *9* — rigid anvil, *10* — velocity transducers, *11* — data processor unit.

In the present study, the use of a relatively long striking pin (60 cm) effectively increased the duration of the incident pulse, contributing to greater plastic deformation during loading. Compared to conventional SHPB systems where shorter striking pins are used (usually less than 30 cm), the elongated striking pin provided sufficient loading time and deformation progression without any significant rise of the strain rate. This configuration, combined with the results of the Taylor test, proved to be particularly suitable for studying the progression of damage in conditions of moderate and low strain rates.

2.2.2. Taylor anvil test

Impact tests were performed using Taylor system shown in Figure 1. The projectile was accelerated by compressed air from a high-pressure chamber (up to 30 atm) separated from the barrel by a bursting membrane. When the membrane ruptured, compressed air pushed a tray made on a 3D printer with a specimen into the barrel (inner diameter: 34 mm). A flange on the muzzle end separated the specimen from the tray before it was hit.

Before hitting the anvil, the leading edge of the cylindrical specimen interrupted two laser beams located at a known distance (the detector response time to the beam is less than $1\,\mu s$). The anvil was made of P6M5 steel (American equivalent — T11302), hardened in oil and then tempered, the surface was polished on a Buehler grinder and lubricated with silicone grease. The dimensions of the sample after the test were measured with a caliper and a micrometer.

For this study, the impact velocities that cause visible defects were selected: 220 m/s — two cracks at an angle of 45° to the contact surface, 243 m/s — multiple radial cracks with a large-size macroscopic cleavage (Figure 2).

3. Results and their discussion

Table 1 shows the methods and test rates of the magnesium alloy specimens studied in the work.

Table 1. Conditions of Mg alloy tests

No.	Test method	Strain rate V, s^{-1}
Initial condition (before deformation)		
1	Instron	10^{-3}
2		10^{-3}
3		10^{-1}
4		10^{-1}
Taylor testing method (v = 219 m/s)		8111.11
1	SHPB	2400
2		1300
4		2130
6		3330
9		5970
10		5500

Figure 2. Fragments of the specimens after the impact tests: *a*) 219 m/s, *b*) 243 m/s).

3.1. Studies of the microstructure of Mg-9Gd-4Y-1Zn-0.5Zr alloy

The microstructure of the magnesium alloy in its initial state is shown in Figure 3. In the longitudinal section, a metallographic texture is visible along the preliminary deformation — extrusion.

3.1.1. Static tests

The microstructure of the magnesium alloy after static tests at the strain rate $10^{-3}\,s^{-1}$ (Figure 4) is similar to that shown in Figure 3 for the initial state. In the longitudinal section, the anisotropy of the structure along the deformation is visible, similar to the metallographic texture in the initial state.

Preserved initial eutectic components of $Mg_5(Gd,Y,Zn)+$ $+(Mg_2Zr+ZrZn_2)$ alloy are observed, fragmented as a result of extrusion (Figure 4, *c*). Grain diversity is observed — large eutectic initial grains and small ones are visible (Figure 4, *d* and *e*), formed during extrusion as a result of dynamic recrystallization.

With the rise of the static deformation rate $10^{-1}\,s^{-1}$, the microstructure of the magnesium alloy changed little. Similar pattern was observed in the initial state and deformation strain rate of $10^{-3}\,s^{-1}$.

3.1.2. Dynamic tests

3.1.2.1. Split Hopkinson pressure bar

With higher load applied to the Hopkinson bar in the test, the number of cracks increases (Figure 5, *a*–*c*), they become more branched, and fracture occurs — separation of the sample into parts.

In addition, local melting followed by crystallization is observed at the highest loading rate (Figure 5, *d* and *e*). Inclusions of zirconium phases are often observed near microcracks, which is confirmed by the EDX method (Figure 6).

Phases enriched in zirconium, as well as, in some cases, phases with a high content of yttrium (up to 47.91%) and gadolinium (up to 29.31 %) have been repeatedly recorded

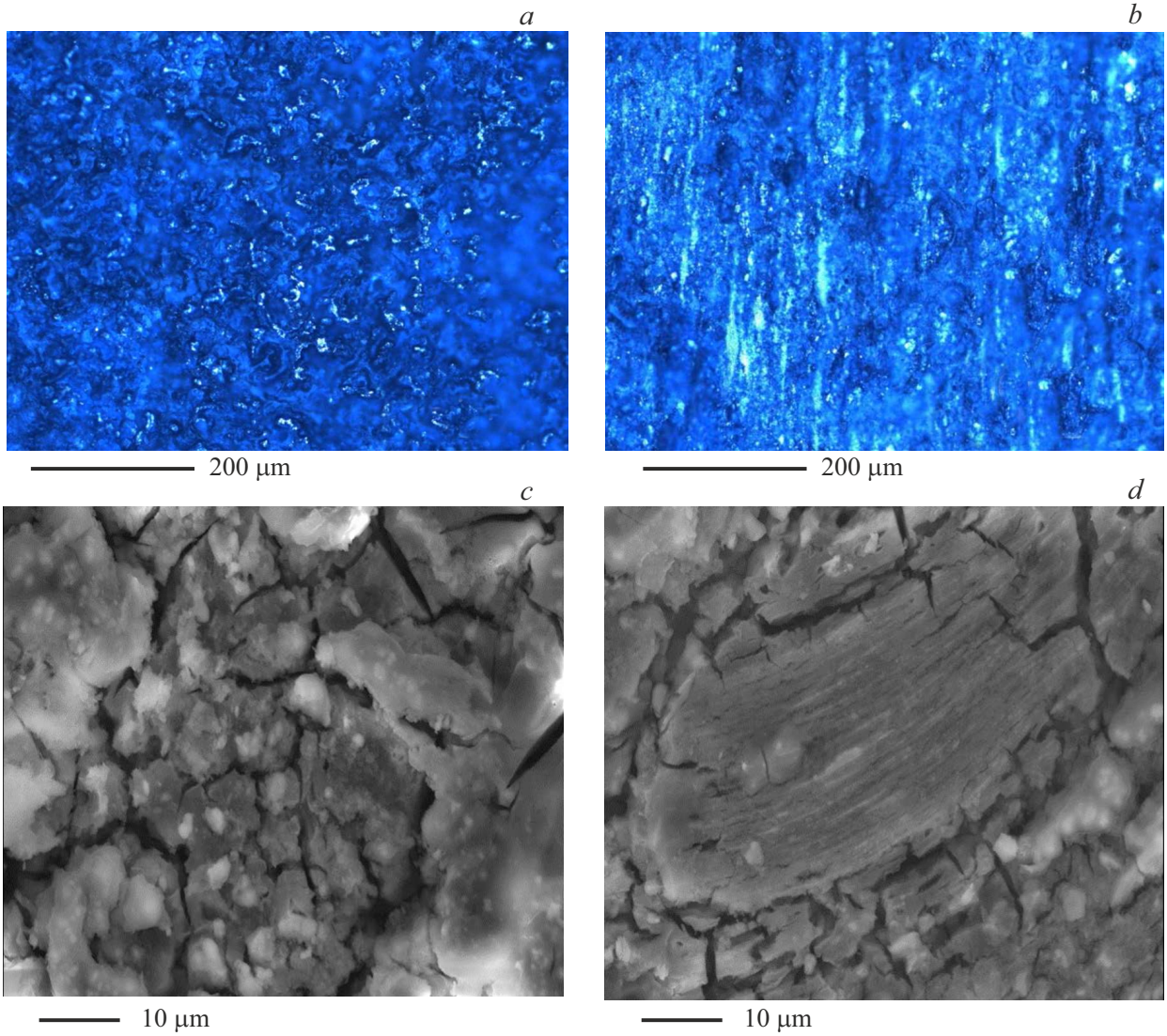

Figure 3. Microstructure of magnesium alloy across and along the bar in its initial state: *a*) ×200 — across the bar, *b*) — ×200 — along the bar. SEM: *c*) across, *d*) along.

in the microcrack region. These areas can contribute to local embrittlement, especially when exposed to high strain rates.

3.1.2.2. Taylor test

Cracks in the cross-section are observed after dynamic loading (Figure 7, *a*). The longitudinal section shows anisotropy (Figure 7, *b, e* and *f*) of the structure along the pre-deformation — extrusion, both in the initial state and in the specimens after quasi-static deformation. The original eutectic components of the alloy are present (Figure 7, *c*), but almost all of them are fragmented.

Grain diversity is observed (Figure 7, *f*) — large grains and small ones formed during extrusion as a result of dynamic recrystallization are visible. Areas with fine grains are observed in the deformed areas, which may be related to both dynamic recrystallization and the effects of extrusion.

3.1.3. Fracture surface analysis

During static fracture, the fracture pattern is predominantly viscous, cup-shaped: the surface contains pits, cup-shaped areas characteristic of this type of fracture. At a rate of 2400 s^{-1}, a visco-brittle fracture mechanism is characteristic: both cup fracture, as well as cleavage and quasi-cleavage are observed.

At higher loading rates, more brittle fracture is observed with areas of cleavage and quasi-cleavage, as well as a stream fracture (Figure 8, *d*) — phases with a high content of yttrium (up to 33.95 %) and gadolinium (up to 19.68 %) were also found in these specimens. As the loading rate increases, the amount of fiber in the fracture (the viscous component) decreases from 91 % in static to 77 % in Hopkinson pressure bar tests and to 49 % in Taylor tests.

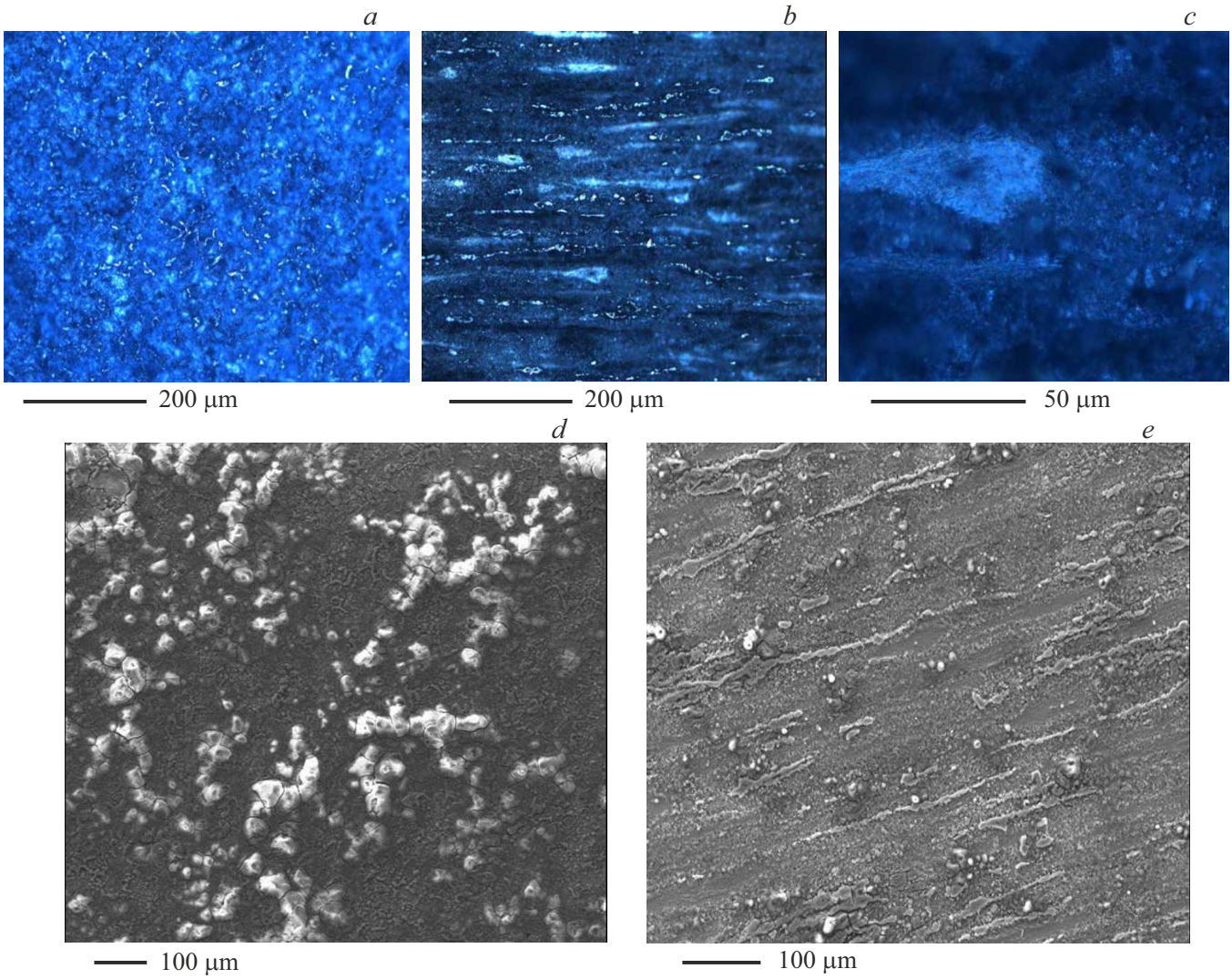

Figure 4. Structure of magnesium alloy after static tests at the strain rate of $10^{-3}\,s^{-1}$. ×200: *a*) across deformation, *b*) along deformation, *c*) along, ×1000. SEM: *d*) across, *e*) along.

3.2. Effect of the strain rate on the characteristics of a magnesium alloy

Figure 9 shows the change in microhardness and grain size depending on the strain rate.

The nature of the change is in antiphase: up to the rate of $2000\,s^{-1}$, the microhardness increases and the grain size declines, then the hardness goes down and the grain size rises, and only after 5000 both, hardness and grain size tend to grow. Up to $5000\,s^{-1}$ the behavior of curves obeys the Hall-Petch law, and only at a higher strain rate this law is violated, as was previously shown by S.A.Atroshenko for steels [7].

The dependence of the stress of the onset of plastic flow or deforming stress on the grain size is consistent with the Hall-Petch ratio:

$$\sigma = \sigma_0 + kd^{-1/2}, \qquad (1)$$

where d — average grain size. This ratio is valid for quasi-static modes and for the characteristics obtained on materials after their dynamic loading. Such characteristics as hardness, ultimate strength and yield strength, as well as the elastic limit in impact-loaded nickel [8] also obey this ratio. However, these material characteristics were measured after impact loading. It is interesting to obtain data on how the strength characteristics of a material change from grain size during impact loading. Such a characteristic can be the spallation strength. In the work [9] it was shown that there is no dependence of the spallation strength on the grain size for steel 1008. The authors of [10] investigated the effect of grain size on the elastic limit of Hugoniot for nickel, iron, aluminum alloy, and copper at short ($10^7\,s^{-1}$) loading pulses. The ratio (1) was found to be not fulfilled. Dependence has the opposite character. In the spallation tests, the specimen is subjected to a flat

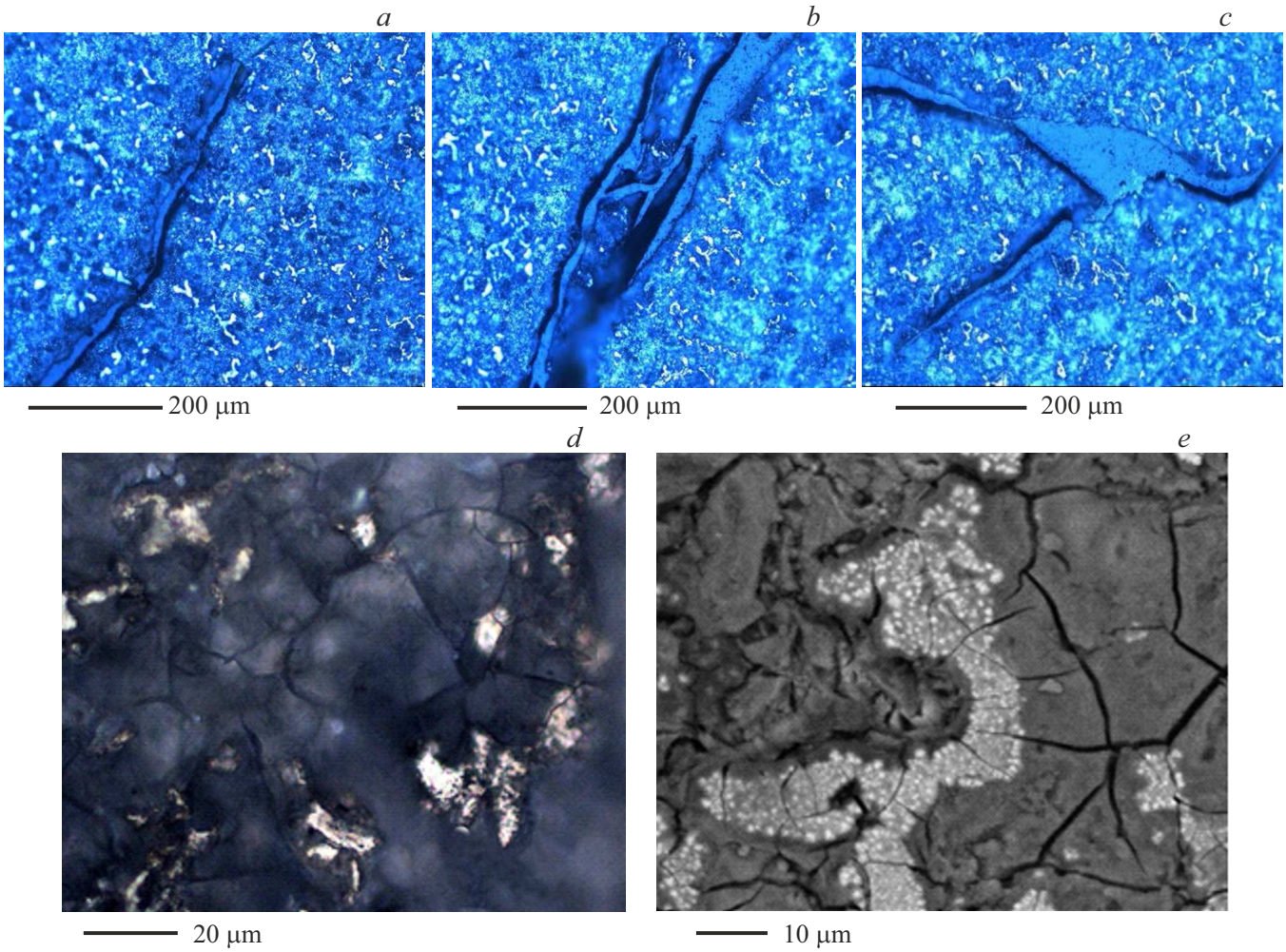

Figure 5. Structure of magnesium alloy after dynamic tests on the split Hopkinson pressure bar: *a*) ×200 ($V = 2400\,\mathrm{s}^{-1}$), *b*) ×200 ($V = 3330\,\mathrm{s}^{-1}$); *c*) ×200 ($V = 5970\,\mathrm{s}^{-1}$); *d*) ×1000 ($V = 5970\,\mathrm{s}^{-1}$); *e*) SEM ($V = 5970\,\mathrm{s}^{-1}$).

Table 2. The effect of grain size on the spallation strength of steel

Steel grade	Speed of loading v, m/s	Spallation strength (speed) W, m/s	Size of grain d, μm
Steel 45	210 253	109 88.5	150 180
Steel 30XH4M	320 361	200 215	8.1 10.3
Steel SP-28	100 321	62 81.5	9.4 32
Steel 12X18H10T	400 447	102 84.5	46 26

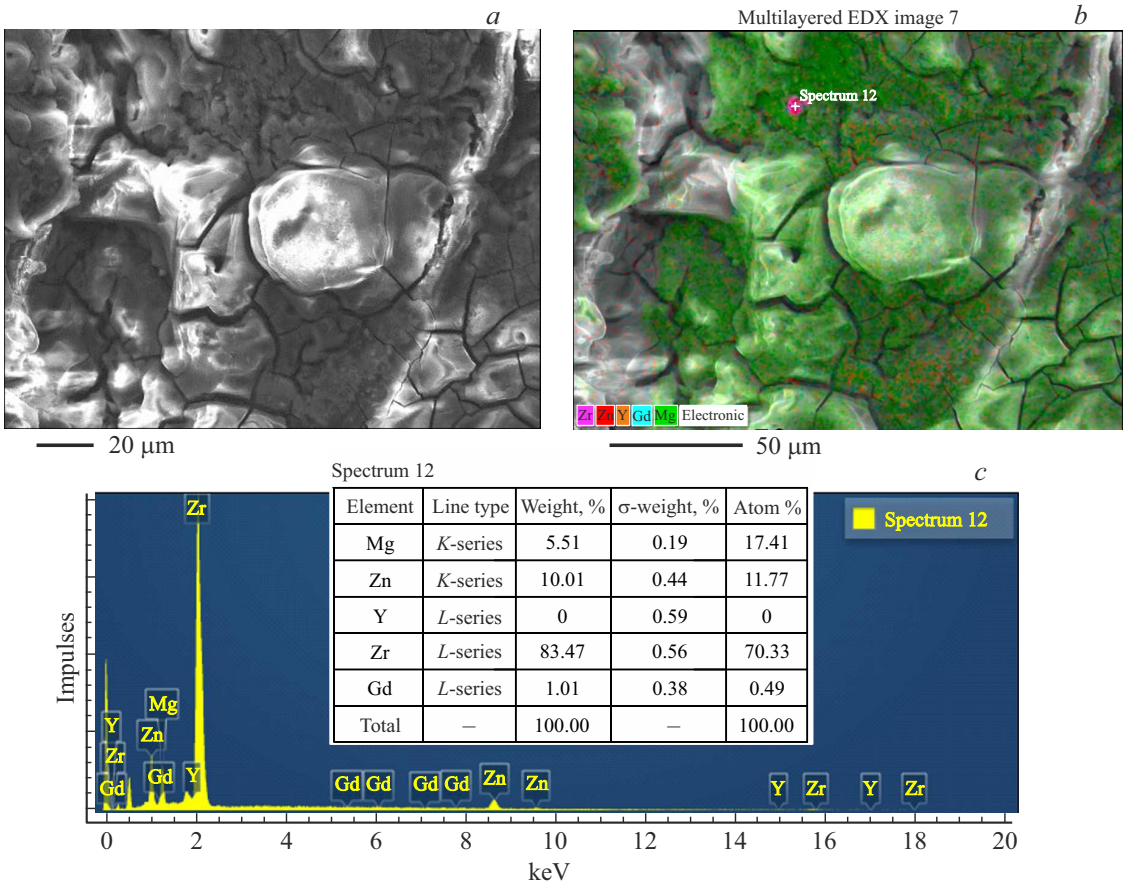

Spectrum 12

Element	Line type	Weight, %	σ-weight, %	Atom %
Mg	*K*-series	5.51	0.19	17.41
Zn	*K*-series	10.01	0.44	11.77
Y	*L*-series	0	0.59	0
Zr	*L*-series	83.47	0.56	70.33
Gd	*L*-series	1.01	0.38	0.49
Total	–	100.00	–	100.00

Figure 6. Formation of cracks in the magnesium alloy and inclusion of Zr phase with the content of 70 % Zr: *a*) SEM ($V = 3330\,\mathrm{s}^{-1}$), *b*) multi-layered EDX image, *c*) spectrum 12 s with the image (*b*).

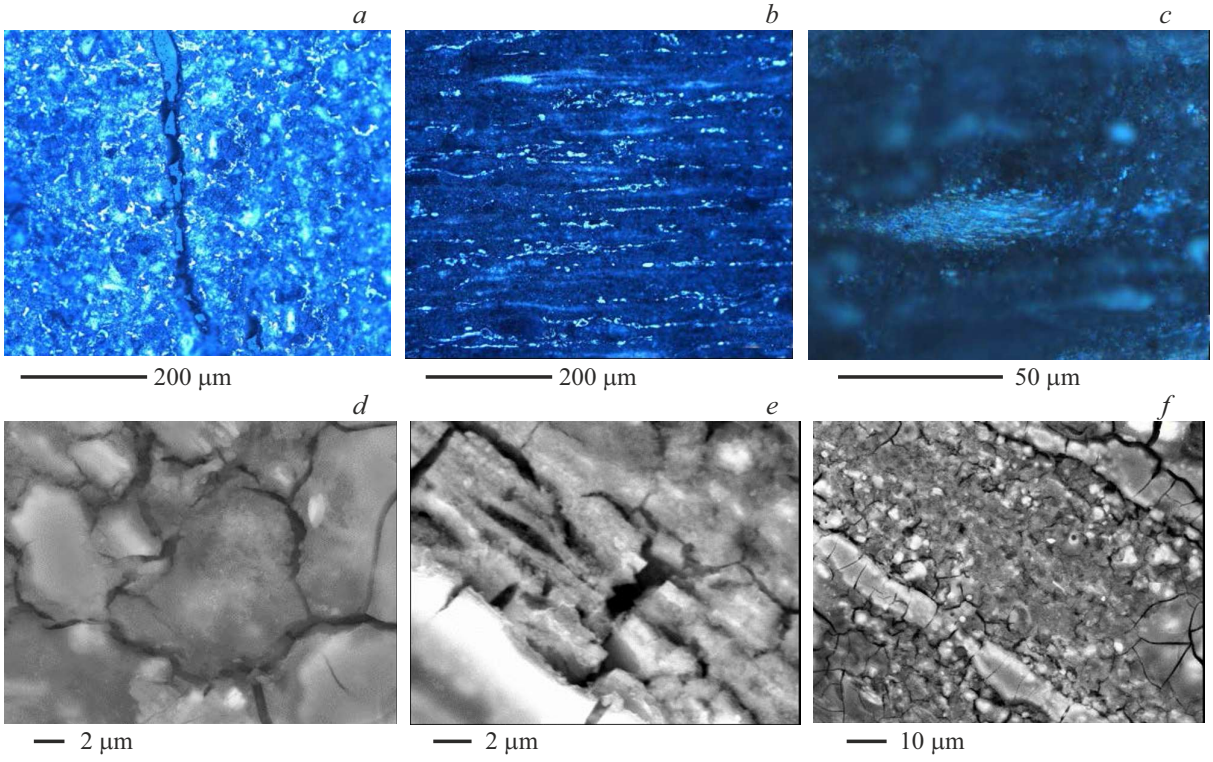

Figure 7. Magnesium alloy microstructure after Taylor's test ($V = 219\,\mathrm{m/s}$). ×200: *a*) across extrusion, *b*) along extrusion. *c*) ×1000 C_DIC. SEM: *d*) across, *e, f*) along.

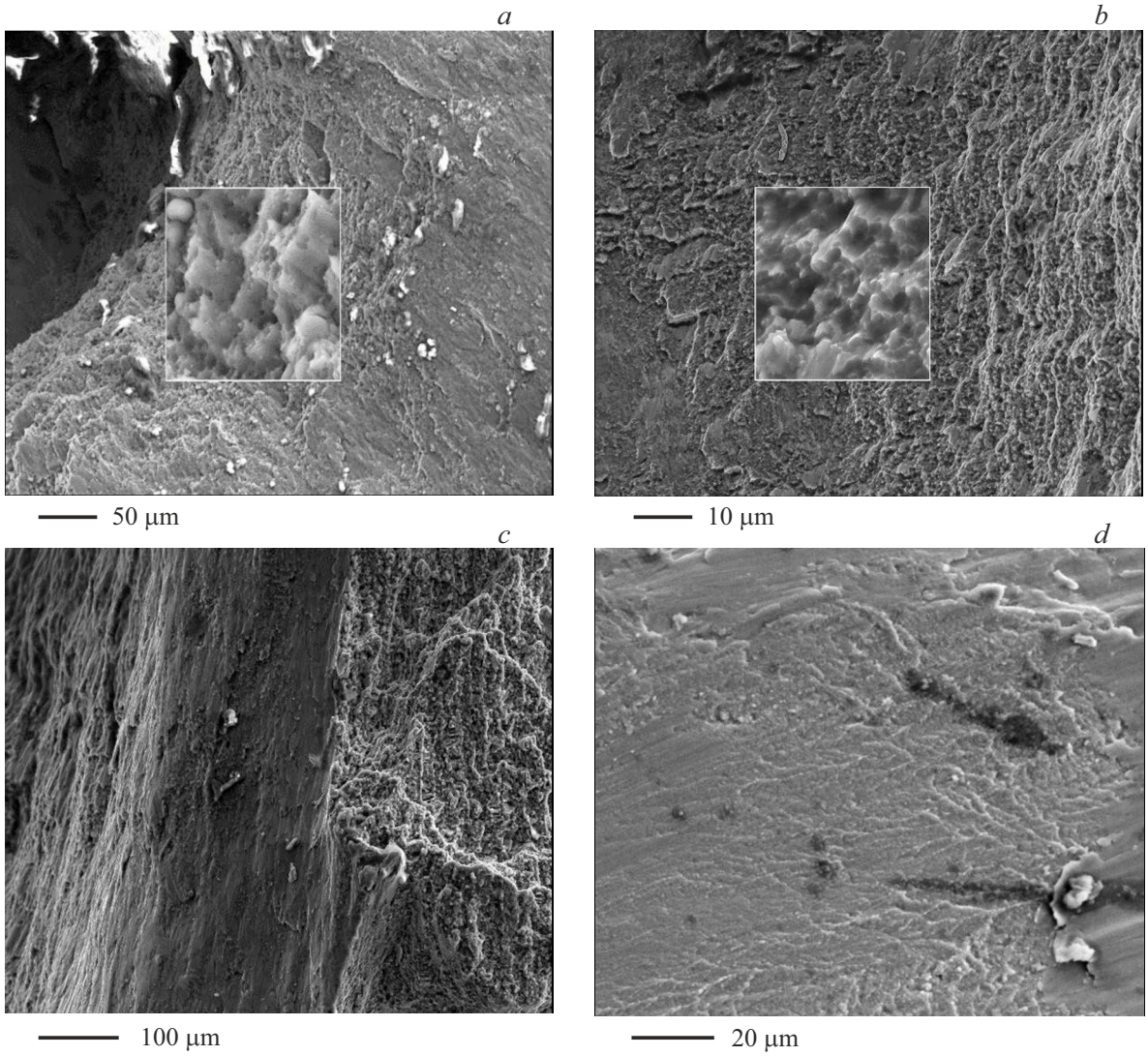

Figure 8. Fracture surface of magnesium alloy: *a*) $V = 10^{-3}\,\mathrm{s}^{-1}$; *b*) $V = 2400\,\mathrm{s}^{-1}$; *c*) $V = 2400\,\mathrm{s}^{-1}$; *d*) $V = 2807\,\mathrm{s}^{-1}$.

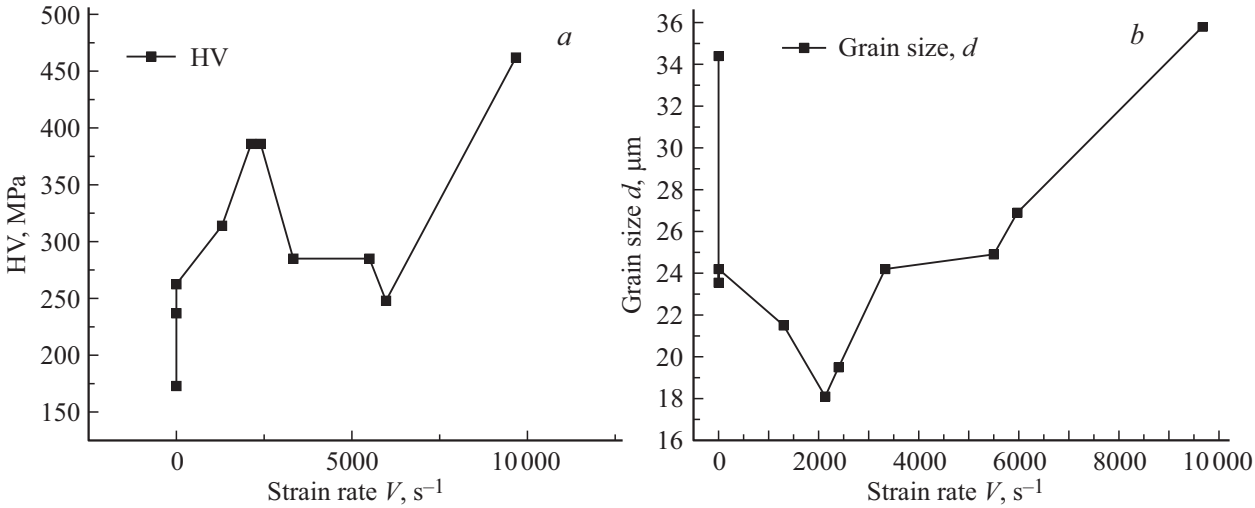

Figure 9. *a*) Microhardness HV and *b*) grain size of the magnesium alloy *d* versus strain rate.

impact, while the specimen and the striking pin are made of steel. When a projectile hits a target, the shock wave propagates into the target and into the striking pin. These waves are reflected from free surfaces and return back to the specimen. When these two unloading waves meet, a stretching wave is formed. If its amplitude exceeds the dynamic strength of the material, a spallation occurs in the specimen. In each experiment, the spallation strength was determined from the time profile of the free surface velocity obtained using a laser interferometer. The target specimens were flat discs with a diameter of 52 mm and a thickness of 5−10 mm. Impact loading was carried out using a 37 mm light gas gun. The rear spallation occurred under conditions of uniaxial deformation when impacted by a steel striking pin with a thickness of 1−3 mm at rates of 100−450 m/s. The results of the experiments are listed in the Table 2.

As can be seen from Table 2, the Hall-Petch ratio is true only for coarse-grained steel 45, hardened by overheating. For all other steels the dependence has the opposite character. This is due to the absence of twinning in 45 steel and the presence of twinning in all other steels. Moreover, the thinner they are and the higher their density, the higher the spallation strength — in steel 30KHN4M.

4. Conclusion

A study of a magnesium alloy in a wide range of loading rates has been carried out.

After quasi-static tests in the longitudinal section, the orientation of the structure along the preliminary deformation is observed — extrusion, as well as fragmented eutectic components of the alloy. Grain diversity is observed: both large initial grains and small grains formed during extrusion as a result of dynamic recrystallization are present.

Areas with fine grains are observed in the deformed areas, which may be related to both dynamic recrystallization and the effects of extrusion. With an increase in the loading rate during Hopkinson pressure bar tests the number of cracks rises, they become more branched, and destruction occurs. The sample is divided into parts, and melting is also locally observed. The presence of microcracks often correlates with inclusions of zirconium phases. Phases enriched in zirconium, as well as, in some cases, phases with high content of yttrium and gadolinium have been repeatedly registered in the fracture region. These areas can contribute to local embrittlement, especially when exposed to high strain rates.

During static fracture, the fracture pattern is predominantly viscous, cup-shaped; at higher loading speeds, more brittle fracture with areas of cleavage and quasi-cleavage is observed.

The nature of the microhardness and grain size change is in antiphase — up to the rate of 2000 s^{-1}, the microhardness rises and the grain size declines, then the hardness goes down and the grain size increases, and only after 5000 s^{-1} both, hardness and grain size tend to grow.

Acknowledgments

The authors express their thanks to the Resource Centers „Nanotechnologies“ and „Center of extreme states of materials and structures“ of the Science Park of Saint-Petersburg State University for the assistance in studying the specimens by method of scanning electron microscopy (SEM) and conducting static tests. Part of the experimental studies of specimens under impact loads was carried out in Mega-Laboratory „Dynamics and Extreme Characteristics of promising nanostructured materials“, created as part of the project 075-15-2022-1114. The authors would like to thank M.M. Nikolaev, a student of the 10th class of „Gorniy“ experimental school for his help in preparing the specimens and conducting the metallographic studies.

Funding

This study was supported financially by the Russian Science Foundation (RSF 22-11-00091). S.A. Atroshenko performed measurements of alloy characteristics with the support of the Ministry of Science and Higher Education of the Russian Federation No. 124041500007-4).

Conflict of interest

The authors declare that they have no conflict of interest.

References

[1] X. Wu, Y. Wang, L. Qiao, J. She, F. Bi. Metals & Mater. Int. **30**, *7*, 2012 (2024). https://doi.org/10.1007/s12540-023-01603-7
[2] X. Wang, Y. Zhao, Y. Huang. Metals & Mater. Int. **29**, *9*, 2556 (2023). https://doi.org/10.1007/s12540-023-01391-0
[3] C. Xu, T. Nakata, G.H. Fan, X.W. Li, G.Z. Tang, L. Geng, S. Kamado. J. Mater. Sci. **54**, *14*, 10473 (2019). https://doi.org/10.1007/s10853-019-03607-4
[4] C. Xu, M.Y. Zheng, K. Wu, E.D. Wang, G.H. Fan, S.W. Xu, S. Kamado, X.D. Liu, G.J. Wang, X.Y. Lv. J. Alloy Compd. **550**, 50 (2013). https://doi.org/10.1016/j.jallcom.2012.09.101
[5] C. Xu, T. Nakata, X. Qiao, M. Zheng, K. Wu, S. Kamado. Sci. Rep. **7**, *1*, 40846 (2017). https://doi.org/10.1038/srep40846
[6] Z.K. Ji, X.G. Qiao, L. Yuan, F.G. Cong, G.J. Wang, M.Y. Zheng. Scripta Materialia **236**, 115675 (2023). https://doi.org/10.1016/j.scriptamat.2023.115675
[7] S.A. Atroshenko. Bull. Am. Phys. Soc. **44**, *2*, 16 (1999).
[8] F. Greulich, L.E. Murr. Mater. Sci. Engr. **39**, *1*, 81 (1978).
[9] A.K. Zurek, P.S. Follansbee, J. Hack. Metall. Trans. A **21A**, 431 (1990).
[10] Yu.V. Sud'enkov, Yu.B. Nikitin. Pisma v ZhTF (in Russian) **19**, *12*, 66 (1993).

Translated by T.Zorina